LETTER

doi:10.1038/nature16514

Covariation of deep Southern Ocean oxygenation and atmospheric CO_2 through the last ice age

Samuel L. Jaccard[1,2], Eric D. Galbraith[3,4,5], Alfredo Martínez-García[6,7] & Robert F. Anderson[8]

No single mechanism can account for the full amplitude of past atmospheric carbon dioxide (CO_2) concentration variability over glacial–interglacial cycles[1]. A build-up of carbon in the deep ocean has been shown to have occurred during the Last Glacial Maximum[2,3]. However, the mechanisms responsible for the release of the deeply sequestered carbon to the atmosphere at deglaciation, and the relative importance of deep ocean sequestration in regulating millennial-timescale variations in atmospheric CO_2 concentration before the Last Glacial Maximum, have remained unclear. Here we present sedimentary redox-sensitive trace-metal records from the Antarctic Zone of the Southern Ocean that provide a reconstruction of transient changes in deep ocean oxygenation and, by inference, respired carbon storage throughout the last glacial cycle. Our data suggest that respired carbon was removed from the abyssal Southern Ocean during the Northern Hemisphere cold phases of the deglaciation, when atmospheric CO_2 concentration increased rapidly, reflecting—at least in part—a combination of dwindling iron fertilization by dust and enhanced deep ocean ventilation. Furthermore, our records show that the observed covariation between atmospheric CO_2 concentration and abyssal Southern Ocean oxygenation was maintained throughout most of the past 80,000 years. This suggests that on millennial timescales deep ocean circulation and iron fertilization in the Southern Ocean played a consistent role in modifying atmospheric CO_2 concentration.

Ice-core and surface-ocean proxy records provide a wealth of evidence supporting a central role of the Southern Ocean in modulating the air–sea partitioning of carbon during ice ages[4,5]. The Southern Ocean could exert a substantial control on the partial pressure of CO_2 (p_{CO_2}), owing to its leverage on the efficiency of the global soft-tissue pump[2] (STP) by which the photosynthetic production, sinking and remineralization of organic matter store dissolved inorganic carbon (DIC) in the ocean interior. At present, vertical exchange of water causes deeply sequestered CO_2 and nutrients to be brought rapidly to the Southern Ocean surface, while iron (Fe) limitation of phytoplankton prevents the exposed nutrients from being entirely fixed back to organic matter before the water sinks again, allowing a net release of CO_2 to the atmosphere. Either decreasing the rate of vertical exchange or enhancing export production would raise DIC concentrations in deep waters, lowering atmospheric CO_2. Higher DIC, in turn, enhances deep water corrosivity, dissolving carbonate ($CaCO_3$) minerals and thereby increasing ocean alkalinity, which produces a further CO_2 drawdown[2].

Phytoplankton productivity in the Subantarctic Zone of the Southern Ocean surface was stimulated during glacial periods by an enhanced supply of Fe-bearing dust, which would have reduced the leakage of CO_2 to the atmosphere, strengthening the overall STP[6,7]. Meanwhile, radiocarbon measurements on deep-sea corals and benthic foraminifera have been interpreted as showing weakened exchange between the surface and the deep Southern Ocean during the Last Glacial Maximum (LGM)[3,8]; if this is correct, such a weakened exchange would have complemented the effect of dust[9]. From the LGM to the Holocene, the combination of dwindling dust inputs and accelerated vertical exchange in the Southern Ocean would have released carbon from the deep sea[5], contributing to the rise of atmospheric CO_2. However, as yet, very little evidence has been reported for STP-driven CO_2 storage in the deep Southern Ocean that extends before the LGM.

Here we report new geochemical observations of changes in the oxygenation of the deep Southern Ocean, chronicling STP carbon storage over the last 80,000 years (80 kyr). DIC storage by the STP, as defined here, is equal to zero in the ocean's surface layer, even though surface waters can contain large amounts of residual carbon inherited from deep waters owing to the slow air–sea exchange of CO_2. This non-equilibrium component in surface waters is referred to as 'disequilibrium DIC' (ref. 10) and would be affected by sea ice, whereas STP DIC storage is independent of sea ice cover. Vertical stable carbon isotope ($\delta^{13}C$) gradients in the Southern Ocean show large changes on glacial–interglacial and millennial (that is, 1–5 kyr) timescales[11]. Although these gradients are influenced by storage of respiratory CO_2 in the deep ocean, they are also susceptible to large disequilibrium effects that may have decoupled $\delta^{13}C$ from DIC storage, since the air–sea equilibration of carbon isotopes is still an order of magnitude slower than for DIC itself[12]. Because dissolved oxygen (O_2) is consumed stoichiometrically during the respiration of sinking organic matter, while being replenished during air–sea exchange an order of magnitude faster than CO_2, it can provide a robust constraint on STP-induced carbon storage.

New measurements were made on two sediment cores raised from 2,800 m and 3,600 m depth at sites just to the north of the Weddell Sea (Methods, Fig. 1), where the bulk of Antarctic Bottom Water (AABW) forms through shelf processes and deep convection[13]. Modern observations show the presence of man-made chlorofluorocarbon-11 (CFC-11) near the core site, unambiguously identifying waters recently ventilated at the Southern Ocean surface (Fig. 1a). Idealized simulations with a fully coupled ocean–atmosphere–biogeochemistry model show that when deep convection in the Weddell Sea is weakened, waters at the core locations become depleted in oxygen, even in a simulation for which North Atlantic Deep Water is somewhat enhanced (Extended Data Fig. 1). At the same time, any change in export production and remineralization rates, including Fe fertilization by abundant glacial dust mobilized from South America during ice ages, would have altered the sinking flux of organic matter to the deep Southern Ocean, thereby changing the consumption rate of oxygen. Prior reconstructions have shown that glacial export fluxes were higher only in the Subantarctic Zone of the Southern Ocean[14], so that the Antarctic Zone sites explored here would have been affected by the southward mixing of oxygen-depleted waters from lower latitudes. Thus, the core sites lie at a critical nexus of the Southern Ocean, where the impact of both deep southern

[1]Institute of Geological Sciences, University of Bern, Bern, Switzerland. [2]Oeschger Center for Climate Change Research, University of Bern, Bern, Switzerland. [3]Department of Earth and Planetary Sciences, McGill University, Montreal, Canada. [4]Institució Catalana de Recerca i Estudis Avançats (ICREA), Barcelona, Spain. [5]Institut de Ciència i Tecnologia Ambientals and Department of Mathematics, Universitat Autonoma de Barcelona, Barcelona, Spain. [6]Geological Institute, ETH Zurich, Zurich, Switzerland. [7]Climate Geochemistry Department, Max Planck Institute for Chemistry, Mainz, Germany. [8]Lamont-Doherty Earth Observatory of Columbia University, Palisades, New York, USA.

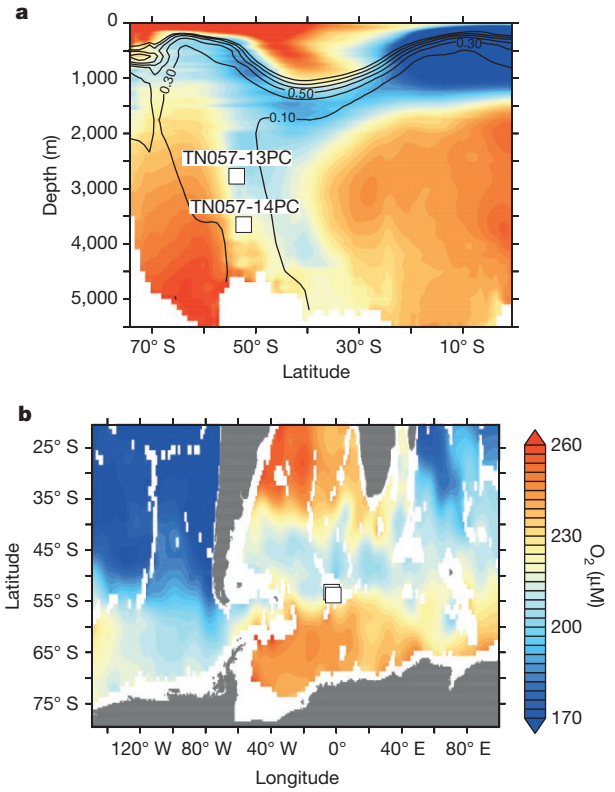

Figure 1 | Modern oceanographic context. a, **b**, Present-day dissolved oxygen concentration[26] is shown on a meridional transect of the South Atlantic, averaged between 25° W and 10° E (**a**) and on a horizontal surface at a water depth of 2,800 m (**b**). Contours in **a** show the concentration of chlorofluorocarbon-11 (CFC-11), in picomoles per kilogram (ref. 27). Both core site locations are bathed by well oxygenated, recently ventilated subsurface water masses and observations suggest that the two sedimentary archives are sensitive recorders with which to monitor changes in deep ocean oxygenation.

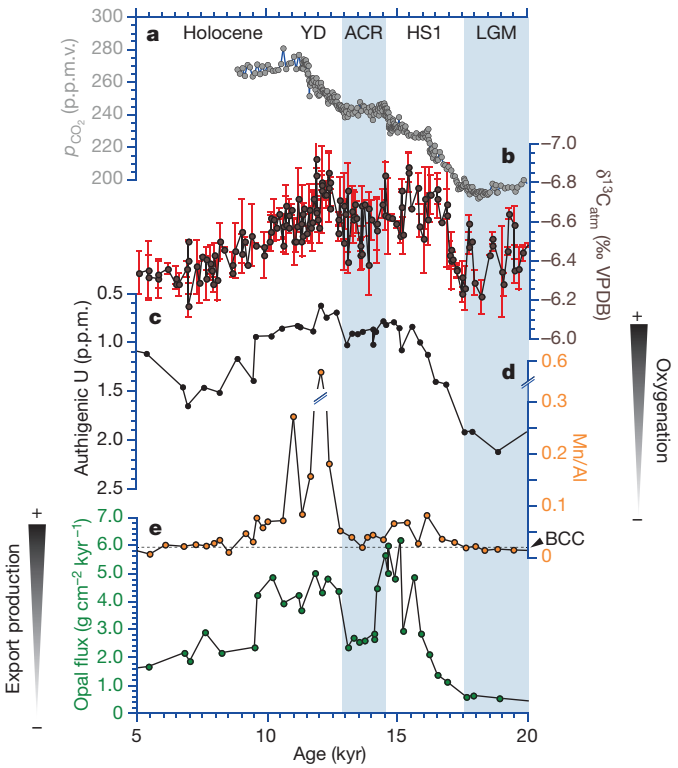

Figure 2 | Palaeoclimatic reconstructions covering the last glacial termination at site TN057-13PC compared with ice core records. **a**, **b**, p_{CO_2} (**a**; ref. 28) and atmospheric $\delta^{13}C$ (**b**; ref. 4, error bars represent the standard deviation of replicate measurements) from Antarctic ice cores. **c**, Sedimentary authigenic U concentrations (reversed scale). **d**, Sedimentary Mn/Al. **e**, ^{230}Th-normalized biogenic opal flux[29]. Shaded intervals highlight cold periods in the Southern Hemisphere. YD, Younger Dryas; ACR, Antarctic Cold Reversal; HS1, Heinrich Stadial 1. The stippled line represents the bulk continental crust (BCC) Mn/Al background value (0.0167; ref. 30). The error (1σ) related to the determination of authigenic U is smaller than the symbol size. p.p.m., parts per million; p.p.m.v., parts per million by volume; VPDB, Vienna Pee-Dee belemnite standard.

ventilation and Fe fertilization on the STP can be recorded by the sedimentary redox state.

The fundamental control on sedimentary redox conditions is the balance between the rate of supply of oxygen from overlying bottom waters and the rate of pore-water oxygen removal associated with respiration, which is regulated by the supply of organic matter. Comparing the sedimentary distribution of redox-sensitive trace metals with biogenic fluxes to the sea floor thus permits these processes to be disentangled, so that relative changes in oxygen concentrations at the water–sediment interface can be inferred. Manganese (Mn) enrichments are typically preserved in well oxygenated sediments, whereas dissolved uranium (U) typically diffuses across the water–sediment interface and subsequently precipitates from pore waters under more reducing conditions (Methods). These mineral precipitates are referred to as authigenic phases. Monitoring the sedimentary distribution of these two metals thus provides sensitivity across the full range of oxygen concentrations typically encountered in the open ocean.

At site TN057-13PC, authigenic U concentrations are highest during peak glacial conditions (LGM in Fig. 2c) and decrease rapidly thereafter, coinciding with the increase in opal flux (Fig. 2e), a proxy for the rain of organic material to the seabed[12] (Extended Data Fig. 2). Higher authigenic U during intervals of lower organic carbon supply to the sea floor can only reasonably be the result of decreased bottom-water oxygen concentrations[15,16], as also observed in prior low-resolution measurements (Extended Data Fig. 3 and Extended Data Table 1), indicating increased storage of remineralized carbon in the deep Southern Ocean during the LGM. Given that the solubility of oxygen in seawater is greater in cold waters, the observation that the deep Atlantic was less well oxygenated during the LGM indicates that the solubility effect on oxygenation was overwhelmed by larger changes in the accumulated utilization of oxygen in the ocean interior[10].

Subsequently, during Heinrich Stadial 1 (HS1, 17.5–14.7 kyr ago), authigenic U accumulation decreased (Fig. 2c) while Mn enrichments rose above the detrital background (Fig. 2d), indicating improved oxygenation of bottom water. This is in striking contrast to the change observed in the deep North Atlantic, where oxygen concentrations fell to their lowest values during HS1, reflecting the reduced input of oxygenated North Atlantic Deep Water[17]. Increased oxygenation during HS1 must have included the effect of decreasing organic matter flux in the Subantarctic Zone, given the rapidly dwindling Fe supply to the surface ocean[6], but the opposing behaviour with the North Atlantic is also consistent with a north–south ventilation seesaw[18]. Importantly, a strong Mn enrichment recurred during the Younger Dryas (12.8–11.5 kyr), when the changes in Fe supply were too small to have altered deep water oxygenation much[7] (Extended Data Fig. 4). Thus, greater oxygenation of deep water at this location during the Younger Dryas event provides evidence for an increased proportion of oxygen-rich AABW relative to oxygen-depleted circumpolar deep water. A northward shift of the circumpolar fronts may have contributed to this increased oxygenation, but if spatial gradients of dissolved oxygen were similar to those that exist today (Fig. 1) then more rapid formation of AABW must have occurred as well, to induce the inferred increase in oxygen. Together, the records imply two phases of STP weakening in the Southern Ocean: the first (HS1) included combined effects of dust

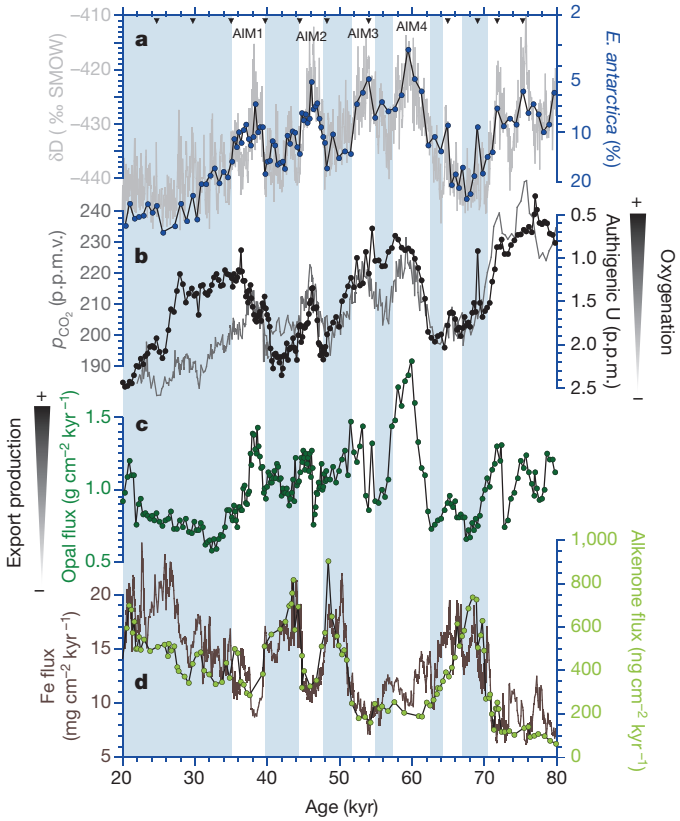

Figure 3 | Palaeoclimatic reconstructions covering the interval MIS2 to MIS5a at site TN057-14PC and Ocean Drilling Program (ODP) site 1090 (42.9° S, 8.9° E, 3,700 m) compared with ice core records. **a**, Relative abundance of diatom *Eucampia antarctica* (blue)—a sea surface temperature proxy—in TN057-14PC (ref. 29) compared to the Antarctic ice core local temperature reconstruction (light grey)[31] on the new AICC2012 age scale[32]. **b**, Ice-core atmospheric p_{CO_2} reconstructions[33,34] (dark grey) and sedimentary authigenic U concentrations at site TN057-14PC (black, reversed scale). **c**, ^{230}Th-normalized biogenic opal flux at site TN057-14PC (ref. 29). **d**, ^{230}Th-normalized Fe (brown) and alkenone (green) fluxes at ODP site 1090 (ref. 6). Triangles indicate the tiepoints used to generate the new version of the TN057-14PC age scale. Shaded intervals highlight cold intervals in the Southern Hemisphere, whereas unshaded intervals correspond to North Atlantic cold periods (Antarctic Isotope Maximum (AIM) 1–4 in the Southern Hemisphere). The error (1σ) related to the determination of authigenic U is smaller than the symbol size. SMOW, Vienna mean ocean water standard.

supply and a north–south seesaw of ventilation, and probably reflected most of the net glacial–interglacial change[10], while the second (Younger Dryas) was dominated by a transient pulse of ventilation alone. These deglacial observations are consistent with the stable carbon isotopic composition of atmospheric CO_2 ($\delta^{13}C_{atm}$) (ref. 4) (Fig. 2b) in suggesting that carbon was removed from the deep Southern Ocean during two episodes of improved deep ocean oxygenation that occurred during HS1 and the Younger Dryas.

Prior to the LGM, atmospheric CO_2 concentrations rose repeatedly by 10–20 parts per million during periods of intense cold conditions in the North Atlantic, while Antarctica warmed. These intervals correspond to perturbations of the Atlantic Meridional Overturning and advances of sea ice in the North Atlantic, similar to HS1 and the Younger Dryas[19], when deep North Atlantic O_2 concentrations plummeted[17]. Our new data show that each of these intervals was also marked by decreasing authigenic U concentrations (Fig. 3b), concurrent with a greater rain of organic detritus to the sea floor (Fig. 3c). Thus, similar to the millennial-timescale changes of the last glacial termination, the oxygenation proxies are consistent with the release of deeply sequestered remineralized carbon to the atmosphere during climate oscillations between 35 kyr and 80 kyr ago. Despite uncertainties in age models and the potential for nonlinear behaviour in authigenic U accumulation, the Pearson's correlation coefficient r^2 between the TN057-14PC authigenic U and the ice-core CO_2 is 0.63 ($P = 10^{-19}$, $n = 89$) over the period 35–80 kyr ago. We note less consistency between 25 kyr and 35 kyr ago, when authigenic U was lower than expected from the p_{CO_2} level; we were unable to find any sedimentological artefact that might have introduced a bias over this interval (Extended Data Fig. 5), and therefore suggest that at this time, during which there was a major expansion of the Northern Hemisphere ice sheets[20], p_{CO_2} was lowered by a mechanism unrelated to the Southern Ocean's control on the STP, although this result should be further tested.

Our results show that carbon storage in the deep Southern Ocean was generally amplified when Antarctica was cold, consistent with arguments based on the similarity of Antarctic temperature and atmospheric CO_2 over glacial cycles. However, the results also highlight a fundamental difference between the glacial–interglacial transition, during which the O_2 changes in the north and south deep Atlantic correlate, and the millennial-timescale changes, for which O_2 changes are antiphased between north and south. This difference can be explained by a contrast in the dynamics of ocean circulation, which were dominated by the bipolar ventilation seesaw on millennial timescales[21] rather than the steady-state adjustment to different CO_2 levels, orbital forcing and ice sheet configuration that determined the glacial–interglacial change[10]. Iron fertilization, caused by enhanced dust input during Antarctic cold phases[6], would have contributed some degree of the observed Southern Ocean STP strengthening during both LGM and millennial-timescale changes. In this light, it may seem remarkable that changes in dust fluxes and deep ventilation were coordinated (Extended Data Table 2), reinforcing their synergistic impacts on the STP.

We suggest that the coordination between ventilation and Fe supply on millennial timescales occurred through a mechanistic link between the two. Model simulations have suggested that a weakening of the Atlantic Meridional Overturning Circulation can lead to enhanced Southern Ocean ventilation via direct ocean circulation changes[21] as well as by forcing a migration in the Southern westerly winds[22]. In addition, it has been shown that a southward shift in the precipitation-bearing Southern Westerlies could initiate the retreat of Patagonian glaciers[23]. We suggest that, owing to this coupling of ocean and atmospheric circulation, millennial-timescale periods of enhanced deep Southern Ocean ventilation generally co-occurred with southward shifts of the Southern Westerlies, which simultaneously caused Patagonian glaciers to retreat, reducing both the production of fine-grained lithogenic material by glacial erosion[24] and the supply of dust by trapping glacial flour in proglacial lakes[25]. Thus, shifts in atmospheric circulation, coupled with changes in the Atlantic Meridional Overturning Circulation, would have caused the intensity of Fe limitation and upwelling to co-vary on millennial timescales, while the intensity of deep convection was altered by both atmospheric and oceanic drivers. These coupled processes, coordinating the input flux of carbon to the deep sea as well as its release by deep convection and upwelling, can explain the remarkable power of the Southern Ocean in modifying the efficiency of carbon storage over millennial timescales, and thereby atmospheric CO_2 levels.

Online Content Methods, along with any additional Extended Data display items and Source Data, are available in the online version of the paper; references unique to these sections appear only in the online paper.

Received 12 March; accepted 27 November 2015.
Published online 3 February 2016.

1. Brovkin, V., Ganopolski, A., Archer, D. & Munhoven, G. Glacial CO_2 cycle as a succession of key physical and biogeochemical processes. *Clim. Past* **8,** 251–264 (2012).
2. Sigman, D. M., Hain, M. P. & Haug, G. H. The polar ocean and glacial cycles in atmospheric CO_2 concentration. *Nature* **466,** 47–55 (2010).
3. Skinner, L. C., Fallon, S., Waelbroeck, C., Michel, E. & Barker, S. Ventilation of the deep Southern Ocean and deglacial CO_2 rise. *Science* **328,** 1147–1151 (2010).

4. Schmitt, J. *et al.* Carbon isotope constraints on the deglacial CO_2 rise from ice cores. *Science* **336,** 711–714 (2012).
5. Martínez-Botí, M. A. *et al.* Boron isotope evidence for oceanic carbon dioxide leakage during the last deglaciation. *Nature* **518,** 219–222 (2015).
6. Martínez-García, A. *et al.* Iron fertilization of the Subantarctic Ocean during the last ice age. *Science* **343,** 1347–1350 (2014).
7. Anderson, R. F. *et al.* Biological response to millennial variability of dust and nutrient supply in the Subantarctic South Atlantic Ocean. *Phil. Trans. R. Soc. Lond. A* **372,** 20130054 (2014).
8. Burke, A. & Robinson, L. F. The Southern Ocean's role in carbon exchange during the last deglaciation. *Science* **335,** 557–561 (2012).
9. Jaccard, S. L. *et al.* Two modes of change in Southern Ocean productivity over the past million years. *Science* **339,** 1419–1423 (2013).
10. Galbraith, E. D. & Jaccard, S. L. Deglacial weakening of the oceanic soft tissue pump: global constraints from sedimentary nitrogen and oxygenation proxies. *Quat. Sci. Rev.* **109,** 38–48 (2015).
11. Ziegler, M., Diz, P., Hall, I. R. & Zahn, R. Millennial-scale changes in atmospheric CO_2 levels linked to the Southern Ocean carbon isotope gradient and dust flux. *Nature Geosci.* **6,** 457–461 (2013).
12. Galbraith, E. D., Kwon, E. Y., Bianchi, D., Hain, M. P. & Sarmiento, J. L. The impact of atmospheric pCO_2 on carbon isotope ratio of the atmosphere and ocean. *Glob. Biogeochem. Cycles* **29,** 307–324 (2015).
13. de Lavergne, C., Palter, J. B., Galbraith, E. D., Bernardello, R. & Marinov, I. Cessation of deep convection in the open Southern Ocean under anthropogenic climate change. *Nature Clim. Change* **4,** 278–282 (2014).
14. Kohfeld, K., Le Quéré, C., Harrison, S. P. & Anderson, R. F. Role of marine biology in glacial-interglacial CO_2 cycles. *Science* **308,** 74–78 (2005).
15. François, R. *et al.* Contribution of Southern Ocean surface-water stratification to low atmospheric CO_2 concentrations during the last glacial period. *Nature* **389,** 929–935 (1997).
16. Frank, M. *et al.* Similar glacial and interglacial export bioproductivity in the Atlantic sector of the Southern Ocean: multiproxy evidence and implications for glacial atmospheric CO_2. *Paleoceanography* **15,** 642–658 (2000).
17. Hoogakker, B. A. A., Elderfield, H., Schmiedl, G., McCave, I. N. & Rickaby, R. E. M. Glacial–interglacial changes in bottom-water oxygen content on the Portugese margin. *Nature Geosci.* **8,** 40–43 (2014).
18. Skinner, L. C., Waelbroeck, C., Scrivner, A. E. & Fallon, S. J. Radiocarbon evidence for alternating northern and southern sources of ventilation of the deep Atlantic carbon pool during the last deglaciation. *Proc. Natl Acad. Sci. USA* **111,** 5480–5484 (2014).
19. Böhm, E. *et al.* Strong and deep Atlantic meridional overturning circulation during the last glacial cycle. *Nature* **517,** 73–76 (2014).
20. Lambeck, K., Rouby, H., Purcell, A., Sun, Y. & Sambridge, M. Sea level and global ice volumes from the Last Glacial Maximum to the Holocene. *Proc. Natl Acad. Sci. USA* **111,** 15296–15303 (2014).
21. Schmittner, A., Brook, E. J. & Ahn, J. in *Ocean Circulation: Mechanisms and Impacts – Past and Future Changes of Meridional Overturning* Vol. 173 *Geophysical Monograph Series* (eds Schmittner, A., Chiang, J. & Hemming, S. R.) 392 (American Geophysical Union, 2007).
22. Chiang, J. C. H., Lee, S.-Y., Putnam, A. E. & Wang, X. South Pacific Split Jet, ITCZ shifts, and atmospheric north-south linkages during abrupt climate changes of the last glacial period. *Earth Planet. Sci. Lett.* **406,** 233–246 (2014).
23. Boex, J. *et al.* Rapid thinning of the late Pleistocene Patagonian Ice Sheet followed migration of the Southern Westerlies. *Sci. Rep.* **3,** 2118 (2013).
24. Herman, F. *et al.* Worldwide acceleration of mountain erosion under a cooling climate. *Nature* **504,** 423–426 (2013).
25. Sugden, D. E., McCulloch, R. D., Bory, A. J.-M. & Hein, A. S. Influence of Patagonian glaciers on Antarctic dust deposition during the last glacial period. *Nature Geosci.* **2,** 281–285 (2009).
26. Garcia, H. E. *et al. Dissolved Oxygen, Apparent Oxygen Utilization, and Oxygen Saturation* Vol. 3 (Government Printing Office, 2010).
27. Key, R. M. *et al.* A global ocean carbon climatology: results from Global Data Analysis Project (GLODAP). *Glob. Biogeochem. Cycles* **18,** GB4031 (2004).
28. Marcott, S. A. *et al.* Centennial-scale changes in the global carbon cycle during the last deglaciation. *Nature* **514,** 616–619 (2014).
29. Anderson, R. F. *et al.* Wind-driven upwelling in the Southern Ocean and the deglacial rise in atmospheric CO_2. *Science* **323,** 1443–1448 (2009).
30. Taylor, S. R. & McLennan, S. M. *The Continental Crust: Its Composition and Evolution. An Examination of the Geochemical Record Preserved in Sedimentary Rocks* (Blackwell Scientific, 1985).
31. Jouzel, J. *et al.* Orbital and millennial Antarctic climate variability over the past 800,000 years. *Science* **317,** 793–796 (2007).
32. Veres, D. *et al.* The Antarctic ice core chronology (AICC2012): an optimized multi-parameter and multi-site dating approach for the last 120 thousand years. *Clim. Past* **9,** 1733–1748 (2013).
33. Ahn, J. & Brook, E. J. Siple Dome ice reveals two modes of millennial CO_2 change during the last ice age. *Nature Commun.* **5,** 3723 (2014).
34. Bereiter, B. *et al.* Mode change of millennial CO_2 variability during the last glacial cycle associated with a bipolar marine carbon seesaw. *Proc. Natl Acad. Sci. USA* **109,** 9755–9760 (2012).

Acknowledgements S.L.J. and A.M.-G. were funded by the Swiss National Science Foundation (grants PP00P2-144811 and PZ00P2_142424, respectively), E.D.G. by NSERC, and R.F.A. by the US NSF. Sediment samples were provided by the core repository at the Lamont-Doherty Earth Observatory. Computational resources were provided to E.D.G. by Compute Canada and the Canadian Foundation for Innovation. We thank C. Buizert, H. Fischer, F. Herman and T. Pedersen for discussions.

Author Contributions S.L.J. and R.F.A. conceived the study and S.L.J. wrote the first iteration of the manuscript. All co-authors provided input to the final version. S.L.J. oversaw the elemental analysis, while R.F.A. supervised the isotopic measurements. E.D.G. provided the climate model outputs and generated the statistical analysis. A.M.-G. refined the age model for core TN057-14PC.

Author Information Reprints and permissions information is available at www.nature.com/reprints. The authors declare no competing financial interests. Readers are welcome to comment on the online version of the paper. Correspondence and requests for materials should be addressed to S.L.J. (samuel.jaccard@geo.unibe.ch).

METHODS

Material and sediment composition. TN057-13PC (53.2° S, 5.1° E, 2,848 m) and TN057-14PC (52.0° S, 4.5° E, 3,648 m) were retrieved from the Atlantic sector of the Southern Ocean, south of the present-day position of the Antarctic Polar Front (Fig. 1). The cores contain diatomaceous ooze sequences with discontinuous carbonate-bearing intervals and occasional ice-rafted debris layers. The deglacial sequence in core TN057-14PC is disturbed and thus was not further considered (Extended Data Fig. 6).

Age model. The TN057-13PC age model is taken, unchanged, from ref. 29. The stratigraphy of sediment core TN057-14PC has been updated on the basis of graphical correlation between the relative abundance of diatom *E. antarctica*[29], a proxy for sea-surface temperature, and EDC deuterium (δD) (ref. 31) expressed on the new AICC2012 age model[32], assuming an in-phase relationship (Fig. 3). Sedimentation rates are high, typically in the range <15–$60\,cm\,kyr^{-1}$, for glacial and peak interglacial intervals, respectively.

Analytical methods. ^{230}Th-normalized fluxes were evaluated as described in ref. 35. Concentrations of U and Th isotopes were determined by isotope dilution inductively coupled plasma mass spectrometry (ICP-MS)[36]. The authigenic U content of each sample was evaluated using the measured ^{238}U and ^{232}Th concentrations using an activity ratio of 0.5 for the detritic endmember[37]. Measured ^{230}Th concentrations were corrected for the detrital contribution using ^{232}Th and for ingrowth produced by authigenic U, and then decay-corrected to the time of deposition to derive ^{230}Th-normalized fluxes. Sedimentary aluminium (Al), manganese (Mn) and barium (Ba) concentrations were measured by inductively coupled plasma optical emission spectroscopy (ICP-OES; Varian Vista Pro) by ALS Minerals, Canada. Precision was better than 2% for replicate measurements. The biogenic fraction of barium—a useful proxy for integrated export production[38]—was determined using a detritic Ba/Al ratio of 0.0067 (ref. 30). The calculations of normative Ba/Al and Mn/Al—the excess Ba and Mn fractions relative to the detrital background, respectively—are based on the assumption that the composition of the Al-bearing phases of the terrigenous material remained constant in space and time. $CaCO_3$ was quantified by coulometric CO_2 determinations assuming no other carbonate-bearing phase was present. Precisions are ±3% of the reported values.

Redox-sensitive metals. The sedimentary distribution of redox-sensitive trace metals can be influenced by a number of factors, including (1) the rate of organic matter delivery to the sea floor, (2) changes in sediment accumulation rate, and (3) changes in bottom-water oxygenation. Comparing the abundance of multiple trace metals (in our case, Mn and U) in sediments with biogenic flux to the sea floor reconstructed using ^{230}Th normalization permits these processes to be distinguished. It follows that relative change of oxygen concentrations at the water–sediment interface can be inferred.

The sedimentary geochemistry of Mn is dominated by the redox control of its speciation, with higher oxidation states (Mn(III) and Mn(IV)) occurring as relatively insoluble oxyhydroxides in well oxygenated environments and the lower oxidation state (Mn(II)) being much more soluble in oxygen-depleted settings[39]. Mn enrichments in the form of Mn-oxide coatings are observed in deep sea sediments where oxic conditions prevail to greater sediment depths as a result of low organic matter respiration rates and well ventilated bottom waters. In sediments that are deposited under reducing conditions, there is no accumulation of Mn oxides and the Mn concentrations of buried deposits are low and entirely controlled by their insoluble detritic fraction. The presence of Mn concentration in excess of what can be expected from the detritic fraction thus suggests that the host sediment must have accumulated under oxygen-replete conditions.

Uranium behaves conservatively in oxygenated seawater and is present as U(VI). One of the primary removal mechanisms for U from seawater is via diffusion across the water–sediment interface of reducing sediments[40]. It appears that for sedimentary redox conditions near those for conversion of Fe(III) to Fe(II) (that is, suboxic conditions), soluble U(VI) is reduced to insoluble U(IV) (ref. 41). This lowers the pore-water U concentration, and dissolved U from the overlying bottom water can diffuse into the sediment along the declining concentration gradient, leading to an enrichment of authigenic (or excess) U in the sediment.

The emplacement of both Mn and U authigenic mineral phases are uncorrelated to ^{230}Th-normalized opal fluxes (Figs 2 and 3, Extended Data Table 2). As a result, we infer that the variability in organic carbon delivery to the sea floor—and its subsequent respiration below the sediment–water interface—was not the primary factor controlling the sedimentary redox conditions.

The sedimentation rates inferred for both sediment cores are high enough to minimize filtering by bioturbation and to prevent post-depositional remobilization of U upon deepening of the sedimentary oxicline. Manganese, on the other hand, is frequently remobilized to the sedimentary pore fluids under reducing conditions. Dissolved Mn can thus migrate in the sedimentary column and (re)precipitate when oxic conditions are encountered[39]. As such, large Mn enrichments primarily reflect a shift from oxygen-depleted to oxygen-replete conditions. The sediment accumulation rate increased across the last glacial termination, potentially affecting trace-metal concentrations. However, both authigenic U and Mn/Al downcore records show opposite behaviours across the deglaciation, suggesting that sedimentary dilution was not the primary controlling factor driving the trace-metal distribution (Extended Data Fig. 7). Furthermore, the comparison between sedimentation rates and authigenic U concentrations in core TN057-14PC (Extended Data Fig. 5) clearly shows that the downcore authigenic U pattern was not dominated by changes in sediment accumulation. We thus posit that the observed authigenic enrichments of both U and Mn were sensitive to changing oxygen levels at the sediment–water interface.

Model simulations. The model simulations were carried out with the Geophysical Fluid Dynamics Laboratory (GFDL) coupled ocean–ice–atmosphere model CM2Mc, with the embedded biogeochemical model BLING[42]. Well equilibrated states of four simulations were used for the plots shown in Extended Data Fig. 1. Extended Data Fig. 1 shows the difference between two simulations with atmospheric CO_2 concentrations of 220 parts per million and LGM ice sheet topography, but different obliquity (axial tilt). Strong convection and AABW production occurs under low obliquity (22°), while moderate convection occurs under high obliquity (24.5°). All other boundary conditions and parameters are identical in the two model runs. The plots were made from 100-year averages over the last century of 3,800-year simulations.

35. François, R., Frank, M., Rutgers van der Loeff, M. M. & Bacon, M. P. ^{230}Th normalization: an essential tool for interpreting sedimentary fluxes during the late Quaternary. *Paleoceanography* **19,** PA1018 (2004).
36. Fleisher, M. Q. & Anderson, R. F. Assessing the collection efficiency of Ross Sea sediment traps using ^{230}Th and ^{231}Pa. *Deep Sea Res. Part II* **50,** 693–712 (2003).
37. Henderson, G. M. & Anderson, R. F. The U-series toolbox for paleoceanography. *Rev. Mineral. Geochem.* **52,** 493–531 (2003).
38. Dymond, J., Suess, E. & Lyle, M. Barium in deep-sea sediments: a geochemical proxy for paleoproductivity. *Paleoceanography* **7,** 163–181 (1992).
39. Calvert, S. E. & Pedersen, T. F. Sedimentary geochemistry of manganese: implication for the environment of formation of manganiferous black shales. *Econ. Geol.* **91,** 36–47 (1996).
40. Klinkhammer, G. P. & Palmer, M. R. Uranium in the oceans: where it goes and why. *Geochim. Cosmochim. Acta* **55,** 1799–1806 (1991).
41. Morford, J. L. & Emerson, S. The geochemistry of redox sensitive trace metals in sediments. *Geochim. Cosmochim. Acta* **63,** 1735–1750 (1999).
42. Galbraith, E. D., Gnanadesikan, A., Dunne, J. P. & Hiscock, M. R. Regional impacts of iron-light colimitation in a global biogeochemical model. *Biogeosciences* **7,** 1043–1064 (2010).
43. Wagner, M. & Hendy, I. L. Trace metal evidence for a poorly ventilated glacial Southern Ocean. *Clim. Past Discuss.* **11,** 637–670 (2015).
44. Yu, J. *et al.* Deep South Atlantic carbonate chemistry and increased interocean deep water exchange during the last deglaciation. *Quat. Sci. Rev.* **90,** 80–89 (2014).
45. Lambert, F., Bigler, M., Steffensen, J. P., Hutterli, M. A. & Fischer, H. Centennial mineral dust variability in high-resolution ice core data from Dome C, Antarctica. *Clim. Past* **8,** 609–623 (2012).
46. Nielsen, S. H. H., Hodell, D. A., Kamenov, G., Guilderson, T. & Perfit, M. R. Origin and significance of ice-rafted detritus in the Atlantic sector of the Southern Ocean. *Geochem. Geophys. Geosyst.* **8,** Q12005 (2007).
47. Kanfoush, S. L. *et al.* Millennial-scale instability of the Antarctic ice sheet during the last glaciation. *Science* **288,** 1815–1819 (2000).
48. Chase, Z., Anderson, R. F. & Fleisher, M. Q. Evidence from authigenic uranium for increased productivity of the glacial Subantarctic Ocean. *Paleoceanography* **16,** 468–478 (2001).
49. Anderson, R. F. *et al.* Late-Quaternary changes in productivity of the Southern Ocean. *J. Mar. Syst.* **17,** 497–514 (1998).
50. Kumar, N. *et al.* Increased biological productivity and export in the glacial Southern Ocean. *Nature* **378,** 675–680 (1995).
51. Martínez-García, A. *et al.* Links between iron supply, marine productivity, sea surface temperature, and CO_2 over the last 1.1 Ma. *Paleoceanography* **24,** PA1207 (2009).
52. Dezileau, L., Bareille, G. & Reyss, J.-L. Enrichissement en uranium authigène dans les sediments glaciaires de l'océan Austral. *C. R. Geosci.* **334,** 1039–1046 (2002).
53. Rosenthal, Y., Boyle, E. A., Labeyrie, L. D. & Oppo, D. Glacial enrichments of authigenic Cd and U in Subantarctic sediments: a climatic control on the elements' oceanic budget? *Paleoceanography* **10,** 395–413 (1995).
54. Bareille, G. *et al.* Glacial-interglacial changes in the accumulation rates of major biogenic components in the Southern Indian Ocean sediments. *J. Mar. Syst.* **17,** 527–539 (1998).
55. Chase, Z., Anderson, R. F., Fleisher, M. Q. & Kubik, P. W. Accumulation of biogenic and lithogenic material in the Pacific sector of the Southern Ocean during the past 40,000 years. *Deep Sea Res. Part II* **50,** 799–832 (2003).
56. François, R., Bacon, M. P., Altabet, M. A. & Labeyrie, L. D. Glacial/interglacial changes in sediment rain rate in the SW Indian sector of Subantarctic waters as recorded by ^{230}Th, ^{231}Pa, U and δ^{15}N. *Paleoceanography* **8,** 611–629 (1993).

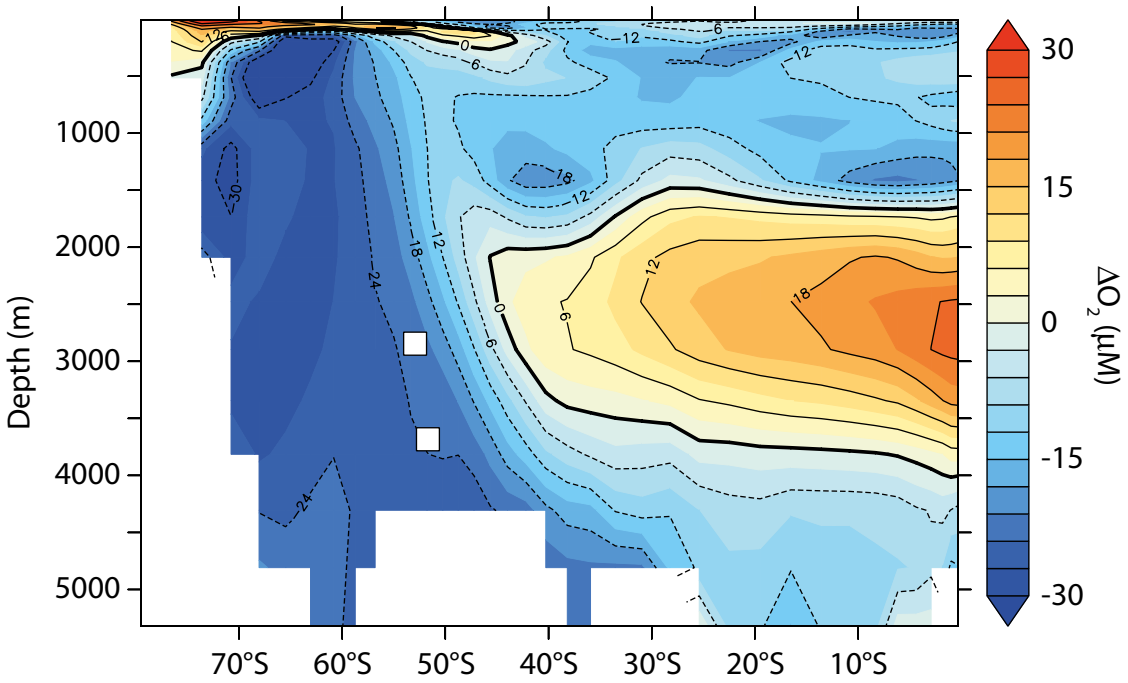

Extended Data Figure 1 | Idealized model experiments illustrating the impact of AABW production on dissolved oxygen relative to the core locations. Shaded contours show the difference in dissolved oxygen (ΔO_2) averaged between 25° W and 10° E, for a coupled model simulation with strong Weddell convection compared to a simulation with moderate Weddell convection (Methods). Squares indicate the location of sediment cores TN057-13PC and TN057-14PC.

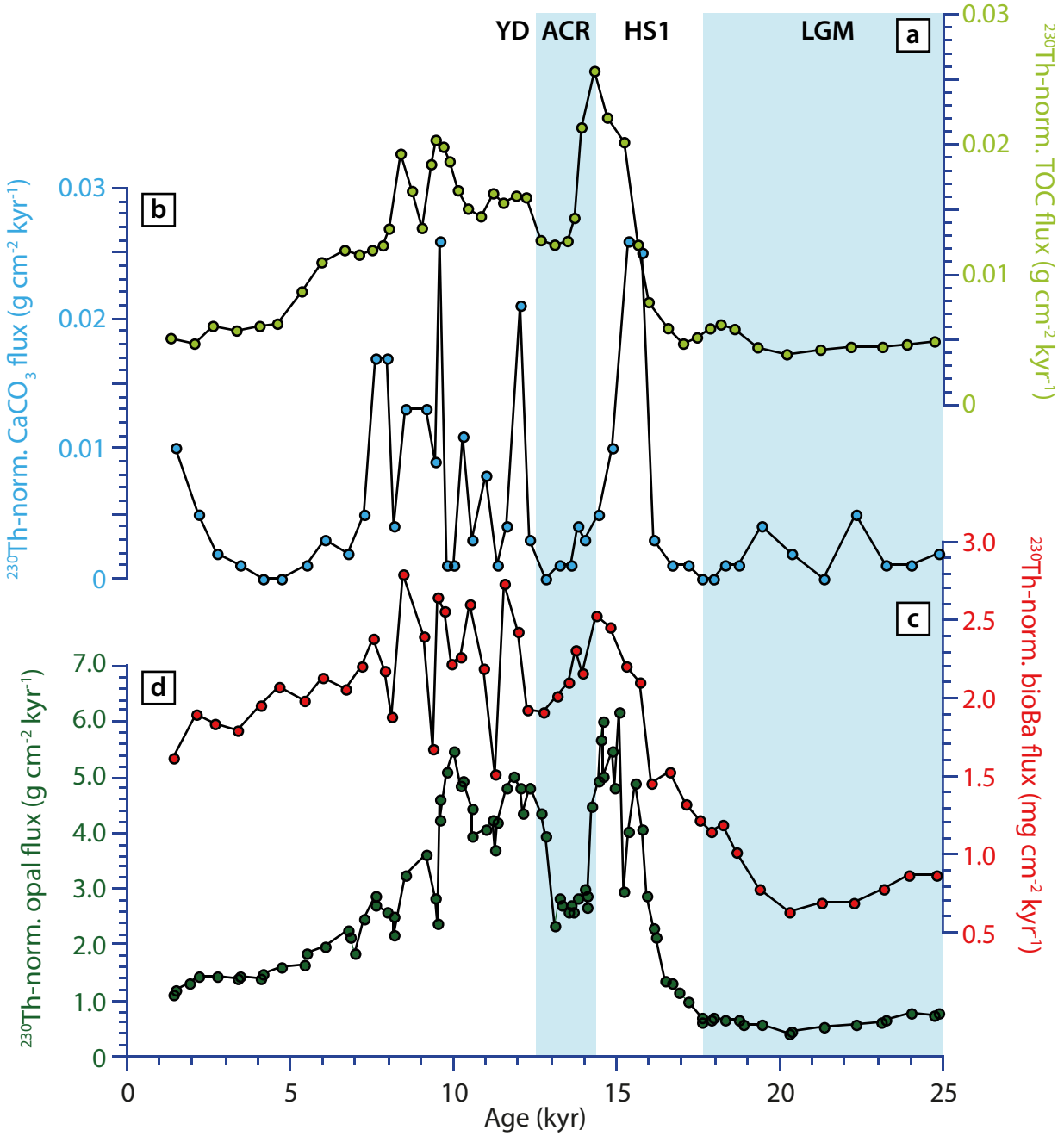

Extended Data Figure 2 | Biogenic particle flux reconstructed by ^{230}Th normalization for four independent proxies covering the last glacial termination at site TN057-13PC. a, ^{230}Th-normalized total organic carbon flux[43]. **b**, ^{230}Th-normalized $CaCO_3$ flux. **c**, ^{230}Th-normalized biogenic barium (bioBa) flux. **d**, ^{230}Th-normalized biogenic opal flux[29]. $CaCO_3$ and bioBa data are from this study. The accumulation of biogenic $CaCO_3$ above glacial background values during HS1 and the YD is consistent with enhanced ventilation of bottom waters during these intervals. Enhanced ventilation of bottom waters would have lowered the regenerated DIC concentration of the bottom water by releasing excess CO_2 to the atmosphere, raising the $[CO_3^{2-}]$ (ref. 44) and calcite saturation state of the bottom water[9] and thus reducing $CaCO_3$ dissolution.

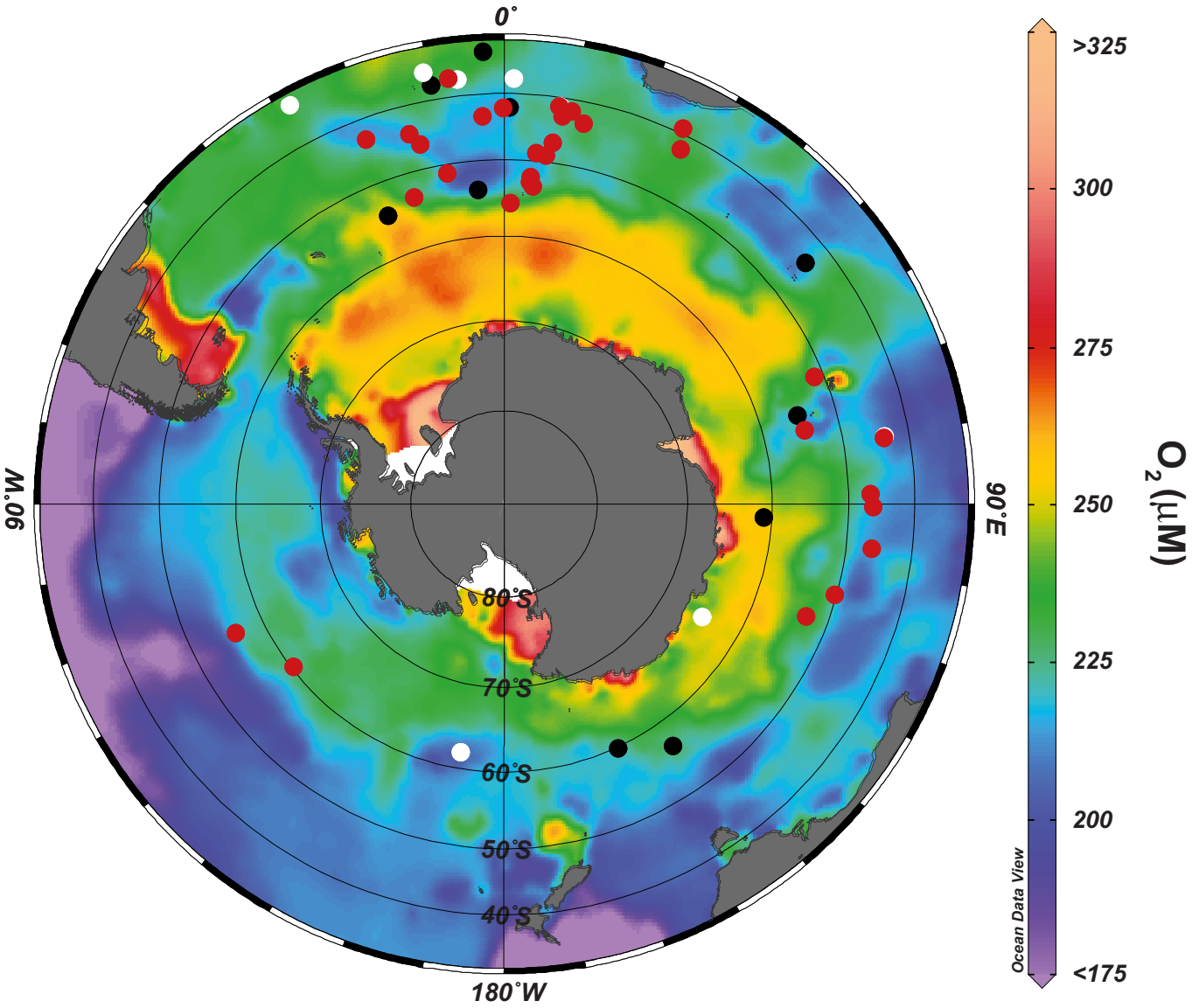

Extended Data Figure 3 | Qualitative changes in oxygenation between the LGM and the Holocene. Red/black dots indicate the location of sedimentary records for which authigenic U concentrations/mass accumulation rates were higher/lower during the LGM when compared to the Holocene, respectively. White dots highlight cores where authigenic U concentrations did not change much between these two intervals (see Extended Data Table 1 for details). Shadings show the modern bottom water dissolved oxygen concentrations[26].

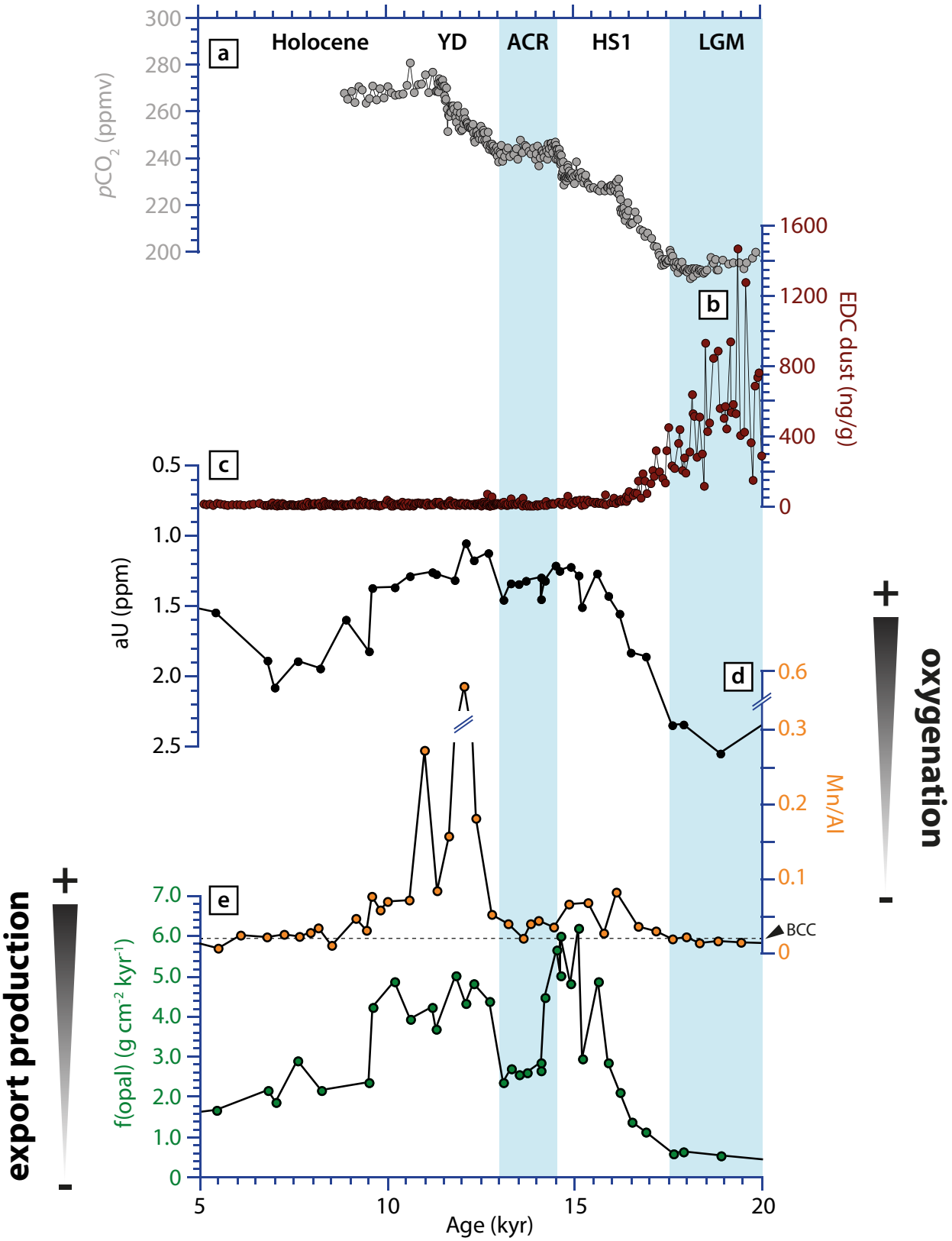

Extended Data Figure 4 | Palaeoclimatic reconstructions covering the last glacial termination at site TN057-13PC compared with ice core records. **a**, Atmospheric p_{CO_2} (ref. 28). **b**, EPICA Dome C (EDC) dust flux[45]. **c**, Sedimentary authigenic U (aU) concentrations. **d**, Sedimentary Mn/Al. **e**, ^{230}Th-normalized biogenic opal flux, f(opal)[29].

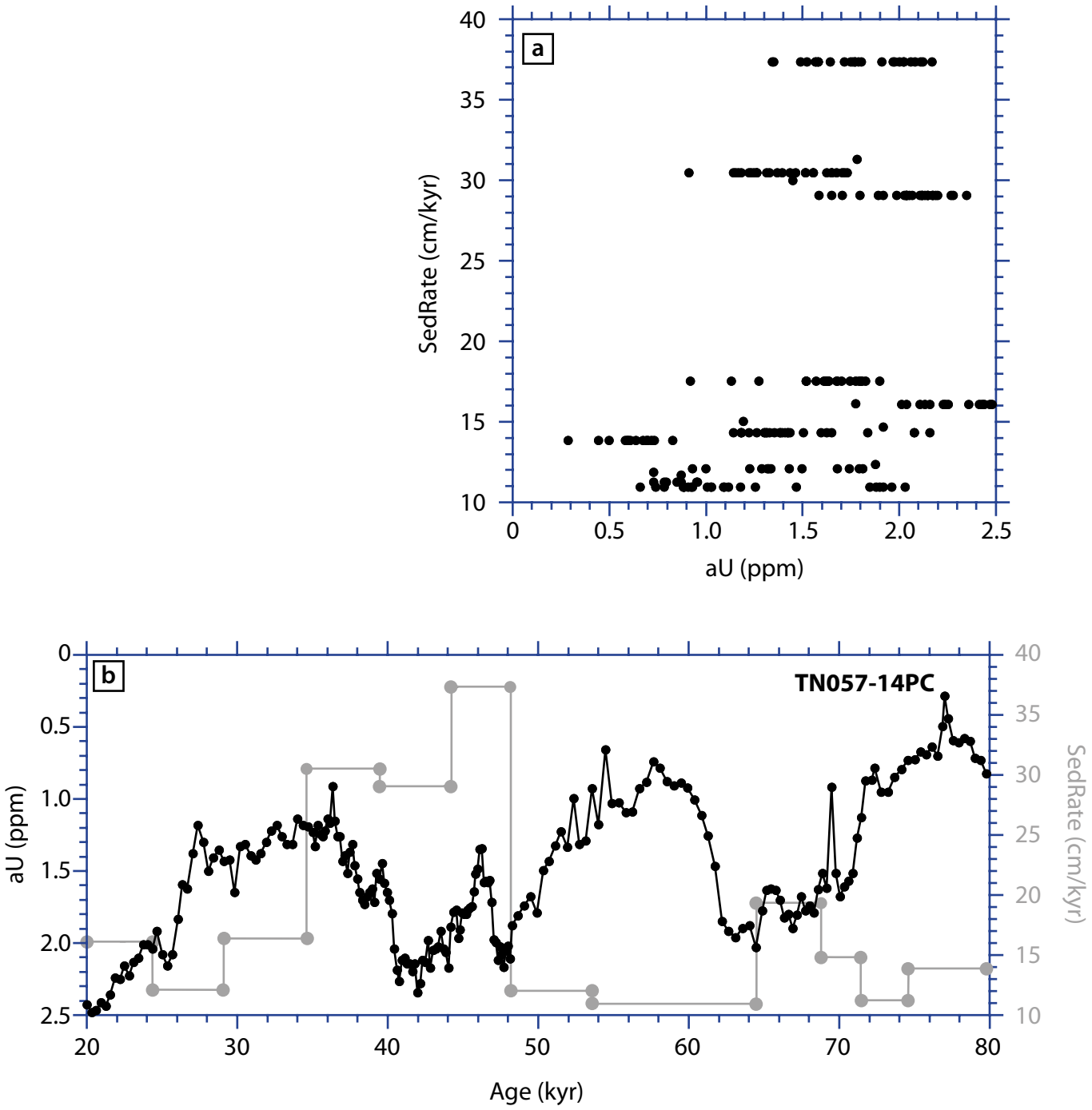

Extended Data Figure 5 | Comparison of bulk sediment accumulation rates and authigenic U concentrations in sediment core TN057-14PC for the interval 20–80 kyr ago. a, Bulk sediment accumulation rates (SedRate). **b**, Authigenic U concentrations.

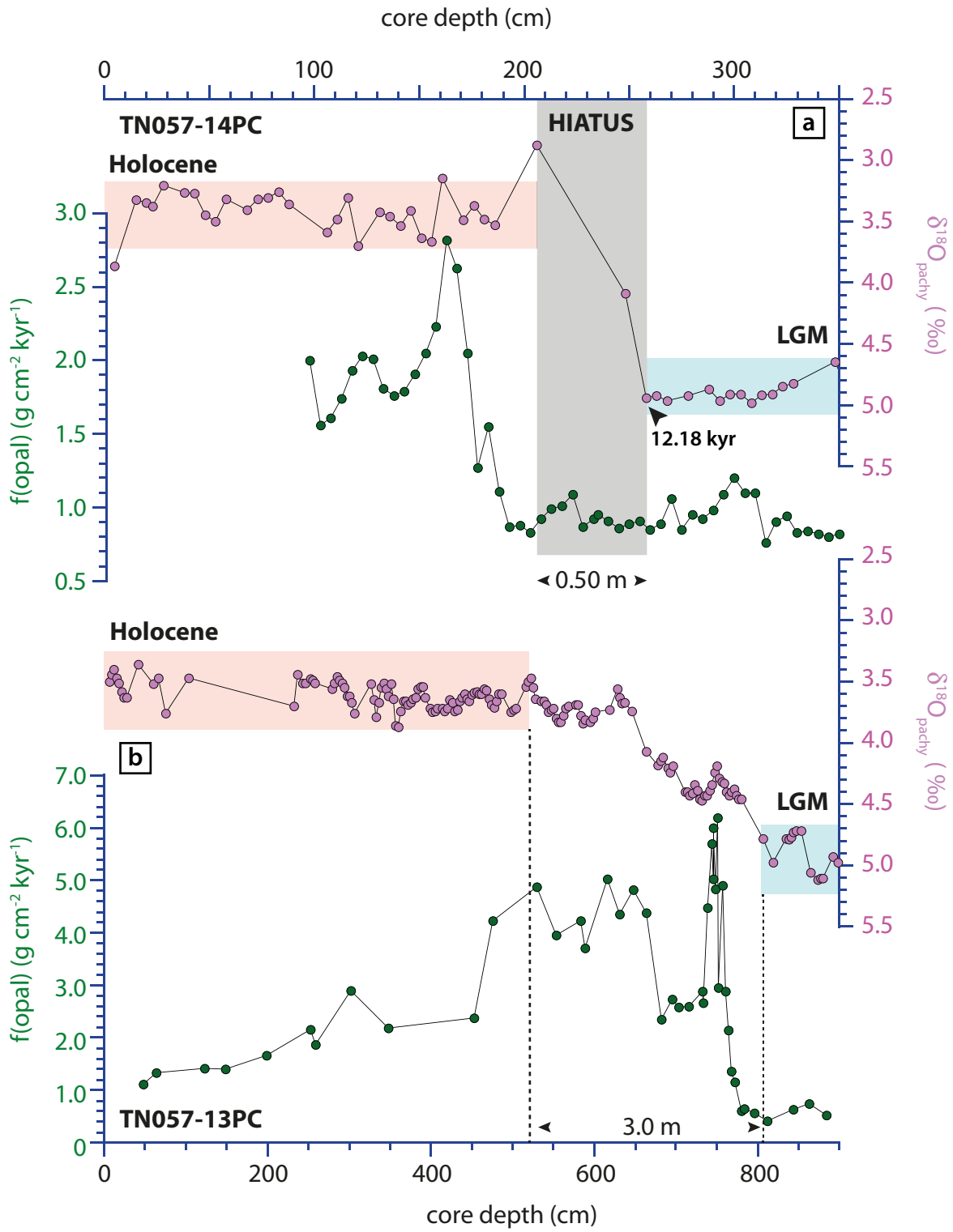

Extended Data Figure 6 | Comparison of the deglacial sequences at sites TN57-14PC and TN057-13PC. a, $\delta^{18}O_{pachy}$ (where 'pachy' refers to the planktonic foraminifera *Neogloboquadrina pachyderma*) (ref. 46) and ^{230}Th-normalized biogenic opal flux[28] in core TN057-14PC. **b**, $\delta^{18}O_{pachy}$ (ref. 47) and ^{230}Th-normalized biogenic opal flux[28] in core TN057-13PC. The grey shading highlights the disturbed portion of core TN057-14PC. The black triangle highlights the presence of planktonic foraminifera deposited during the Younger Dryas (that is, 12.18 kyr ago; ref. 46), which have been mixed down into late LGM sediments after the hiatus occurred.

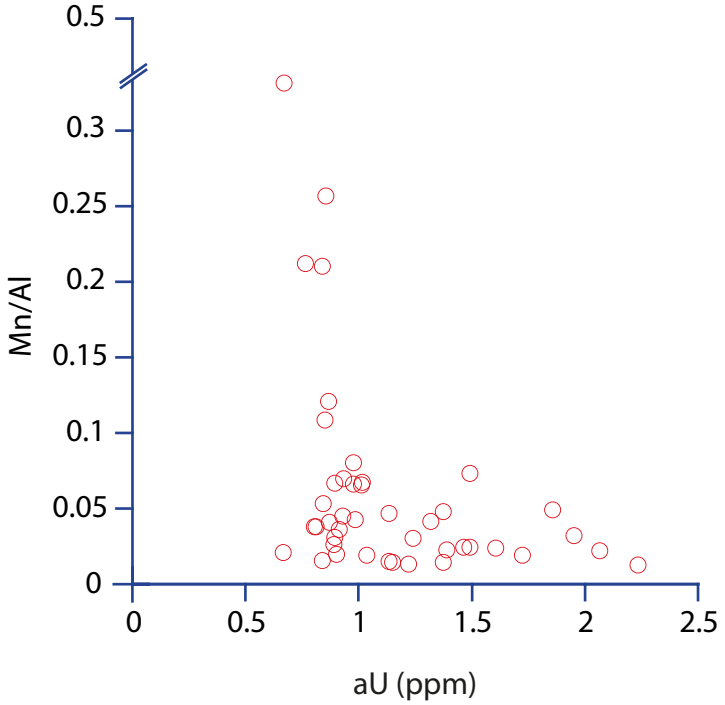

Extended Data Figure 7 | Cross-plot of Mn/Al and authigenic U across the last glacial termination in sediment core TN057-13PC.

Extended Data Table 1 | Available Southern Ocean low-resolution records permitting reconstruction of the authigenic U Holocene–LGM gradient compiled from the literature

Core	Latitude	Longitude	Depth (m)	References
Sedimentary records showing *higher* aU concentration/accumulation during the LGM (18-22kyr) than the Holocene (0-10kyr)				
VM27-196	-36.33	-7.57	1,106	Chase et al., 01 (ref. 48)
RC12-267	-38.68	25.45	4,144	Anderson et al., 98 (ref. 49)
TN057-21	-41.13	7.82	4,981	Kumar et al., 95 (ref. 50)
RC11-83	-41.60	9.72	4,718	Chase et al., 01 (ref. 48)
VM34-157	-41.95	26.42	3,636	Anderson et al., 98 (ref. 49)
VM22-109	-41.97	-0.25	733	Chase et al., 01 (ref. 48)
ODP1090	-42.60	8.50	3,700	Martinez-Garcia et al., 09 (ref. 51)
RC15-94	-42.90	-20.85	3,762	Kumar et al., 95 (ref. 50)
VM22-108	-43.18	-3.25	4,171	Kumar et al., 95 (ref. 50)
PS2082	-43.21	11.73	4,610	Frank et al., 00 (ref. 16)
RC11-120	-43.52	79.87	3,193	Anderson et al., 98 (ref. 49)
PS2498-1	-44.15	-14.49	3,783	Anderson et al., 14 (ref. 7)
MD88-770	-46.00	96.50	3,290	Dezileau et al., 02 (ref. 52)
MD88-769	-46.10	90.10	3,420	Rosenthal et al., 95 (ref. 53)
RC15-93	-46.10	-13.21	2,714	Anderson et al., 98 (ref. 49)
MD94-104	-46.50	88.10	3,460	Dezileau et al., 02 (ref. 52)
PS1754	-46.77	7.61	2,471	Frank et al., 00 (ref. 16)
RC13-254	-48.57	5.12	3,636	Kumar et al., 95 (ref. 50)
PS1756	-48.73	6.71	3,787	Frank et al., 00 (ref. 16)
MD88-772	-50.00	104.90	3,240	Bareille et al., 98 (ref. 54)
RC11-78	-50.86	-9.86	3,115	Chase et al., 01 (ref. 48)
MD80-304	-50.93	67.43	1,930	Rosenthal et al., 95 (ref. 53)
RC13-271	-51.98	4.51	3,634	Kumar et al., 95 (ref. 50)
PS1768	-52.60	4.48	3,270	Frank et al., 00 (ref. 16)
MD88-773	-52.90	109.87	2,460	Bareille et al., 98 (ref. 54)
RC11-77	-53.05	-16.45	4,098	Anderson et al., 98 (ref. 49)
TN057-13PC	-53.20	5.10	2,848	*this study*
MD84-552	-54.40	75.83	1,780	Dezileau et al., 02 (ref. 52)
PS1772	-55.46	1.17	4,135	Frank et al., 00 (ref. 16)
E11-2	-56.07	-115.09	3,111	Chase et al., 03 (ref. 55)
E20-10	-60.22	-127.05	4,474	Chase et al., 03 (ref. 55)
Sedimentary records showing *lower* aU concentration/accumulation during the LGM than the Holocene				
VM24-221	-32.03	-2.82	4,204	Chase et al., 01 (ref. 48)
RC12-294	-37.26	-10.10	3,308	Chase et al., 01 (ref. 48)
TN057-20	-42.10	0.60	1,312	Chase et al., 01 (ref. 48)
MD84-527	-43.83	51.33	3,269	Francois et al., 93 (ref. 56)
RC13-259	-53.88	-4.93	2,677	Kumar et al., 95 (ref. 50)
RC11-76	-54.38	-22.13	5,229	Anderson et al., 98 (ref. 49)
E33-22	-54.93	-120.00	2,744	Chase et al., 03 (ref. 55)
MD84-551	-55.10	73.30	2,230	Bareille et al., 98 (ref. 54)
MD84-787	-56.40	145.30	3,020	Bareille et al., 98 (ref. 54)
E27-23	-59.62	155.24	3,215	Anderson et al., 09 (ref. 29)
KR8830	-61.00	93.20	4,300	Bareille et al., 98 (ref. 54)
E17-9	-63.08	-135.00	4,849	Chase et al., 03 (ref. 55)
Sedimentary records showing no significant difference in aU concentration/accumulation between the LGM and the Holocene				
VM24-240	-31.73	-28.20	4,327	Chase et al., 01 (ref. 48)
VM24-229	-34.45	-10.60	4,202	Chase et al., 01 (ref. 48)
VM27-197	-36.68	-6.27	4,089	Chase et al., 01 (ref. 48)
RC13-243	-36.90	1.33	4,790	Chase et al., 01 (ref. 48)
VM14-65	-41.00	8.00	4,825	Chase et al., 01 (ref. 48)
MD94-102	-43.50	79.80	3,205	Bareille et al., 98 (ref. 54)
NBP9802-6	-61.88	-169.98	3,245	Chase et al., 03 (ref. 55)
NBP9802-5	-63.11	-169.74	2,940	Chase et al., 03 (ref. 55)
MD88-791	-64.70	119.50	3,150	Bareille et al., 98 (ref. 54)

Records from references 7, 16, 29 and 48–56.

Extended Data Table 2 | Statistical correlation between sedimentary proxies for the interval 20–82 kyr ago

	1090 f(Fe)	1090 f(alk)	TN057 aU	TN057 f(opal)	pCO_2
1090 f(Fe)					
1090 f(alk)	.62; 0.0000				
TN057 aU	.52; 0.0000	.64; 0.0000			
TN057 f(opal)	.24; 0.0000	.18; 0.0000	.13; 0.0000		
pCO_2	.71; 0.0000	.57; 0.0000	.58; 0.0000	.32; 0.0000	

^{230}Th-normalized Fe and alkenone fluxes were measured at ODP site 1090 (ref. 6). Sedimentary U concentrations and ^{230}Th-normalized opal fluxes[29] were measured at TN057-14PC; p_{CO_2} levels were measured on Antarctic ice[33,34]. Numbers in red represent the correlation coefficient, r^2; the blue numbers indicate the P values, which are less than 10^{-20} in all cases.